

Spin-orbit interactions mediated negative differential resistance in a quasi-two-dimensional electron gas with finite thickness

E. Nakhmedov^{1,2}, O. Alekperov², and R. Oppermann¹

¹*Institut für Theoretische Physik, Universität Würzburg, Am Hubland, D-97074 Würzburg, Germany*

²*Institute of Physics, Azerbaijan National Academy of Sciences, H. Cavid str. 33, AZ1143 Baku, Azerbaijan*

(Dated: December 5, 2018)

Effects of the spin-orbit interactions on the energy spectrum, Fermi surface and spin dynamics are studied in structural- and bulk-inversion asymmetric quasi-two-dimensional structures with a finite thickness in the presence of a parabolic transverse confining potential. One-particle quantum mechanical problem in the presence of an in-plane magnetic field is solved numerically exact. Interplay of the spin-orbit interactions, orbital- and Zeeman-effects of the in-plane magnetic field yields a multi-valley subband structure, typical for realization of the Gunn effect. A possible Gunn-effect-mediated spin accumulation is discussed.

PACS numbers: 72.25.Dc, 75.70.Tj, 75.76.+j, 71.70.Ej

One of the major goals of modern electronics is the search for new spin-involved functionalities [1] in solid state nanoscale devices. Electric field controlled Rashba spin-orbit (SO) coupling [2], which is originated from large potential gradient on the semiconductor/insulator interface of quantum wells and MOSFETs in the presence of macroscopic structural inversion asymmetry (SIA), is a promising tool [3] in a realization of spin transport devices. On the other hand, special semiconduction materials with a bulk inversion asymmetry (BIA) in their crystalline structure produce so-called Dresselhaus SO interaction [4], which interplays with Rashba interaction yielding unusual physical effects [5, 6].

Different experimental techniques have been developed recently to control a coupling of spin to the electric field [7–9]. An efficient \hat{g} -tensor modulation resonance, observed in a parabolic $Al_xGa_{1-x}As$ quantum well [7] with varying Al content $x = x(z)$ across the well, provided an opportunity to manipulate electron spins by means of various electron spin resonance type techniques. In-plane magnetic field in all of these experiments seems to be rather favorable to get a pronounced spin resonance. On the other hand, gate voltage control of spin dynamics in practical devices was shown [10] to be reasonable only for a finite thickness of the electron gas. SO interactions in a 2D electronic system produce an effective in-plane field, which results in an drift-driven in-plane spin polarization [11]. External in-plane magnetic field appears to be not always algebraically summed with SO induced effective field and results in a surprising out-of-plane spin polarization [12], which was observed in strained $n - InGaAs$ film [8]. On the other hand Hanle precession of optically oriented 2D electrons in $GaAs$ [13] can be well described by algebraic addition of these fields. All these facts show nontrivial effects of in-plane magnetic field on spin dynamics in quasi-2D systems.

In this paper we show that an interplay of Rashba and Dresselhaus SO interactions in a quasi-two-dimensional (quasi-2D) electron gas with finite thickness results in a

multi-valley ('N'-shaped) energy dispersion in the presence of an in-plane magnetic field. The obtained energy-momentum relation looks like those existing in $GaAs$ and InP -type materials of the transferred-electron devices, where negative differential resistance and Gunn microwave current oscillations take place. Finite thickness of the electron gas gives rise to transverse-quantized levels with Rashba-Dresselhaus spin-split subbands in each level. The in-plane magnetic field removes degeneration in the anticrossing points of different subbands, opening a magnetic field-controlled gap at these points. Barrier height between the valleys in the 'N'-shaped energy-momentum relation and the valley curvatures seem to be controlled by Rashba- and Dresselhaus SO coupling constants, the in-plane magnetic field strength and Landé factor. The dependence of the energy spectrum on the magnetic field shows strongly non-linear and non-monotonic behavior even in weak field strengths.

The single particle Hamiltonian of the system in the effective mass approximation is written as

$$\hat{H} = \frac{\mathbf{P}^2}{2m^*} + \frac{m^*\omega_0^2 z^2}{2} - eE_g z + \hat{H}_{so} + \frac{1}{2}g\mu_B\sigma\mathbf{B}, \quad (1)$$

where $\mathbf{P} = \mathbf{p} - \frac{e}{c}\mathbf{A}$ is an electron momentum in the presence of a vector-potential \mathbf{A} , m^* and e are the electronic effective mass and charge, respectively; E_g is a strength of the gate electric field. A parabolic potential with a frequency ω_0 , characterizing the electron gas thickness, does not produce SO interactions, and is chosen in Eq.(1) to confine the electron gas in z -direction. Since Rashba SO interaction in the conduction band of a semiconductor is determined by the electric field in the valence band rather than by that in the conduction band [14], the parabolic confinement approximation neglects a small interface contribution to Rashba SO coupling constant. The last term in Eq.(1) is Zeeman splitting energy in the external magnetic field \mathbf{B} with $\hbar\omega_z = g\mu_B B/2$, where $\mu_B = \frac{e\hbar}{2m_0}$ is the Bohr magneton of a free electron with mass m_0 , g is the effective Landé factor, and

$\sigma = \{\sigma_x, \sigma_y, \sigma_z\}$ are the Pauli spin matrices. \hat{H}_{so} in Eq.(1) contains Rashba term as well as Dresselhaus term with characteristic parameters α and β , correspondingly

$$\hat{H}_{so} = \frac{\alpha}{\hbar}(\sigma_x P_y - \sigma_y P_x) + \frac{\beta}{\hbar}(\sigma_x P_x - \sigma_y P_y). \quad (2)$$

The electronic wave function $\Psi(x, y, z)$ can be expressed in the form $\Psi(x, y, z) = e^{ik_x x + ik_y y} \psi_{\uparrow(\downarrow)}^{(\sigma)}(z)$ for a magnetic field aligned along x -axes $\mathbf{B} = \{B, 0, 0\}$ under the gauge $\mathbf{A} = \{0, -Bz, 0\}$. In the absence of the SO interactions and Zeeman term, Hamiltonian becomes diagonal and the equations for ψ_{\uparrow} and ψ_{\downarrow} are reduced to the oscillator equation $\hat{H}_0 \psi_n^{(0)}(z) = E_n \psi_n^{(0)}$ with real wave function $\psi_n^{(0)}(z) = (\sqrt{\pi} 2^n n!)^{-1/2} \exp[-(z - z_0)^2 / (2a_B^2)] H_n((z - z_0)/a_B)$ and the energy spectrum $E_n = \hbar\omega(n + 1/2) - \frac{\hbar^2 k^2}{2m^*} + \frac{(\hbar k_y \omega_B - eE_g)^2}{2m^* \omega^2}$, where $z_0 = \frac{eE_g - k_y \hbar \omega_B}{m^* \omega^2}$, $a_B = (\hbar/m^* \omega)^{1/2}$, $\omega = (\omega_B^2 + \omega_0^2)^{1/2}$, $\omega_B = eB/m^* c$, $k = (k_x^2 + k_y^2)^{1/2}$, and $H_n(z)$ is the Hermite polynomial. General solutions are chosen as linear combinations of $\psi_n^{(0)}(z)$

$$\psi_{\sigma}(z) = e^{-\frac{(z-z_0)^2}{2a_B^2}} \sum_{n=0}^{\infty} \frac{a_n^{\sigma}}{\sqrt{a_B \sqrt{\pi} 2^n n!}} H_n\left(\frac{z - z_0}{a_B}\right), \quad (3)$$

where $\sigma = \uparrow, \downarrow$. By putting Eq.(3) into Schrödinger equation one gets the matrix equations $\hat{\mathbf{N}}_{\sigma} \mathbf{a}^{\sigma} = 0$ for the vectors $\mathbf{a}^{\sigma} = \{a_0^{\sigma}, a_1^{\sigma}, a_2^{\sigma}, \dots\}$. $\hat{\mathbf{N}}_{\sigma}$ with $\sigma = \uparrow, \downarrow$ are square pentadiagonal matrices of infinite order with non-zero entries $N_{i,j}^{\sigma} \neq 0$ only if $|i - j| \leq 2$, and $\hat{\mathbf{N}}_{\uparrow} = (\hat{\mathbf{N}}_{\downarrow})^*$. The energy spectrum has to be found from the secular equation, by equating the determinant of the matrix $\hat{\mathbf{N}}$ to zero. The infinite pentadiagonal matrix is truncated down to the first n rows and n columns, and the roots of its determinant are found by numeric methods. All parameters in our numeric calculations, shown below with tilde, are done dimensionless in the unit of the characteristic frequency ω_0 of the confining potential or in the length scale $l_0 = (\hbar/m^* \omega_0)^{1/2}$, which is a measure of the electron gas thickness.

Energy spectrum. The solutions of the $n \times n$ determinant converge very rapidly as n increases. The energy dispersion for the first three transverse quantized levels ($n=3$) is depicted in Fig.1 for different values of the SO coupling constants and the magnetic field. In the absence of the in-plane magnetic field and one of the SO coupling constant, the energy spectrum $E_n(k_y)$ is described by the well-known two symmetric parabolas in each transverse-quantized level (dashed (green) curves in Fig.1a). An external gate electric field $\tilde{f}_g \equiv eE_g l_0 / (\omega_0 \hbar)$ coherently shifts the energy subbands. Non-zero k_x component of the momentum splits spin-up and spin-down spectra at $k_y = 0$. The energy spectrum becomes asymmetric along momentum- and energy-axes if $\tilde{\alpha} \equiv \alpha / (\hbar \omega_0 l_0) \neq 0$, $\tilde{\beta} \equiv \beta / (\hbar \omega_0 l_0) \neq 0$ and $k_x \neq 0$. Energy spectra corresponding to the same transverse-quantized level with

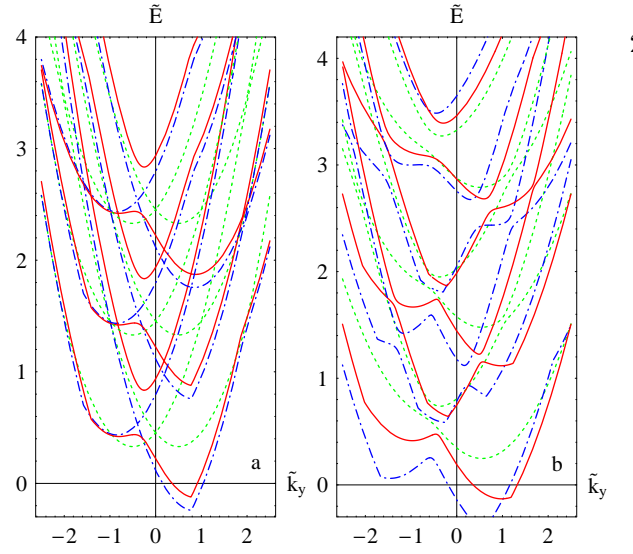


FIG. 1: (Color online) Dependence of the energy spectrum on Rashba- and Dresselhaus SO coupling constants as well as on the orbital- and spin-effects of the in-plane magnetic field. E vs. k_y is shown (a) in the absence of the magnetic field at $\tilde{k}_x = 0$, $\tilde{f}_g = 0.3$, $\tilde{\alpha} = 0.5$, $\tilde{\beta} = 0$ by dashed (green) curves; $\tilde{k}_x = 0.4$, $\tilde{f}_g = 0$, $\tilde{\alpha} = \tilde{\beta} = 0.6$ by dot-dashed (blue) curves and $\tilde{k}_x = 0.4$, $\tilde{f}_g = 0$, $\tilde{\alpha} = 0.8$, $\tilde{\beta} = 0.4$ by solid (red) curves; (b) under the in-plane magnetic field $\tilde{\omega}_B = 0.7$, $\tilde{g} = 0.2$ and $\tilde{k}_x = 0.2$, $\tilde{\beta} = 0.4$ but for different values of $\tilde{\alpha}$ and \tilde{f}_g : $\tilde{\alpha} = 0.4$, $\tilde{f}_g = 0$ by dashed (green) curves, $\tilde{\alpha} = 1.2$, $\tilde{f}_g = 0.3$ by dot-dashed (blue), and $\tilde{\alpha} = 0.9$, $\tilde{f}_g = 0$ by solid (red) curves.

opposite spin orientations split at the intersection point for $\alpha \neq \beta$, whereas they do not split at the intersection point for $\alpha = \beta$. Nevertheless, anticrossing of the energy spectra corresponding to different levels persists irrespective of the values of α and β . Fig.1b describes the dependence of E_n on k_y in the presence of the in-plane magnetic field $\tilde{\omega}_B \equiv \omega_B / \omega_0$, Zeeman splitting $\tilde{g} \equiv gm^* / (4m_0)$ and $\tilde{k}_x \neq 0$ for different values of the SO coupling constants. The magnetic field seems to remove the degeneracy at the anticrossing points, and to open a gap, which increases with magnetic field. Although the Zeeman splitting strongly modifies the energy levels in the presence of only Rashba SO coupling, shifting the parabolas bottoms along k_y and splitting the energies of spin-up and spin-down electrons, it does not change the levels symmetry in the presence of only Dresselhaus SO coupling (dot-dashed (blue) curves in Fig.1b). The same picture is obtained for the energy dispersion along k_x under the similar conditions given in Fig.1b but with the replacements $k_x \leftrightarrow k_y$ and $\alpha \leftrightarrow \beta$.

The dependence of the energy spectrum on the in-plane magnetic field under different momentum components and SO coupling constants is given in Fig.2a for zero Landé factor and in Fig.2b for a non-zero Landé factor, $\tilde{g} = 0.2$. The energy spectrum in both cases displays considerably nonlinear and non-monotonic behavior even under weak magnetic fields, when $0 < \tilde{\omega}_B < 1$. The magnetic field splits the spectrum at the anticrossing points. The energy dispersion in the negative magnetic field is

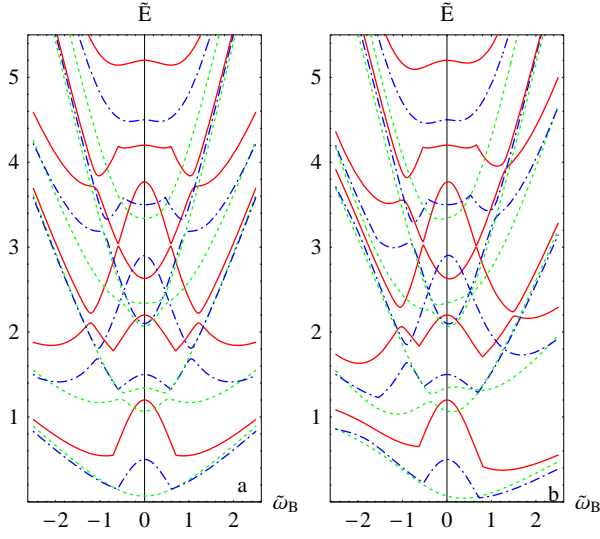


FIG. 2: (Color online) Dependence of the energy spectrum on the in-plane magnetic field (a) in the absence $\tilde{g} = 0$ and (b) in the presence $\tilde{g} = 0.2$ of Zeeman splitting at $\tilde{f}_g = 0$. The parameters $\tilde{k}_x = 0.4$, $\tilde{k}_y = 0.5$, $\tilde{\alpha} = 0.6$, and $\tilde{\beta} = 0.4$ correspond to dotted (green) curve. Dashed (blue) and solid (red) curves depict the cases $\tilde{k}_x = 0.2$, $\tilde{k}_y = 1.4$, $\tilde{\alpha} = 0.8$, $\tilde{\beta} = 0.4$ and $\tilde{k}_x = 0.4$, $\tilde{k}_y = 1.8$, $\tilde{\alpha} = 0.6$, $\tilde{\beta} = 0.4$ respectively.

exactly the same as the dispersion in the positive magnetic field but with reversed in sign the Landé factor.

Fermi surface. Influence of different SO interactions and in-plane magnetic field on the Fermi surface is shown in Fig.3 for electrons, resided the first transverse-quantized level. The dimensionless energy is fixed in the middle of the two adjacent transverse levels $\tilde{E}_F \equiv E_F/(\hbar\omega_0) = 1.0$. In the presence of only one SO interaction the Fermi surface is symmetrically splitted at $\omega_B = 0$ into two surfaces of spin-up and spin-down electrons even under non-zero gate voltage. Fermi surfaces become strongly anisotropic for $\alpha \neq 0$ and $\beta \neq 0$ due to shifting of two circles away from each other in both k_x and k_y directions. If $\alpha \neq \beta$, the circles corresponding to spin-up and spin-down electrons split at the intersection points. Nevertheless they do not split at the intersection points if Rashba and Dresselhaus constants are equal each other, $\alpha = \beta$. Gate voltage increases the anisotropy, but it does not split the Fermi surface at the intersection points for $\alpha = \beta$. Instead, in-plane magnetic field removes a degeneracy at the intersection points.

Spin-Gunn effect. Multi-valley energy dispersion, discussed above, allow us to suggest an existence of negative differential resistance and spin-Gunn effect [15] in a quasi-2D electron gas in the presence of SO interactions. Assume that the Fermi level crosses the second transverse-quantized level in the energy-momentum dispersion, shown in Fig.1b with solid (red) curve under the conditions $\tilde{k}_x = 0.2$, $\tilde{\alpha} = 0.9$, $\tilde{\beta} = 0.4$, $\tilde{\omega}_B \equiv B/B_0 = 0.7$, and $\tilde{g} = 0.2$. In order to estimate $\tilde{\alpha}$, $\tilde{\beta}$, $B_0 = m^*c\omega_0/e$ and the electron gas thickness $l_0 = \sqrt{\hbar/m^*\omega_0}$, we use $\alpha \sim 1 \times 10^{-8} \text{ eV} \cdot \text{cm}$, and $\beta \sim 0.4 \times 10^{-8} \text{ eV} \cdot \text{cm}$, as well as $\omega_0\hbar \sim 10 \text{ meV}$, [16], which yield $l_0 = 10.6 \text{ nm}$

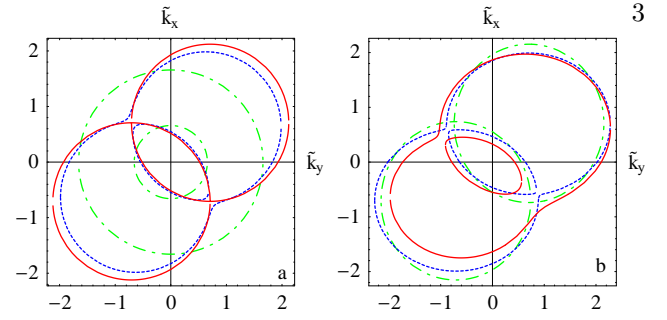


FIG. 3: (Color online) Fermi surface of electrons in the first transverse-quantized level. (a) Dot-dashed (green) curves correspond to $\tilde{\alpha} = 0.5$, $\tilde{\beta} = 0$, $\tilde{f}_g = 0.3$, dashed (blue) curves to $\tilde{\alpha} = 0.5$, $\tilde{\beta} = 0.4$, $\tilde{f}_g = 0$ and solid (red) curves to $\tilde{\alpha} = \tilde{\beta} = 0.5$, $\tilde{f}_g = 0$ in the absence of magnetic field $\tilde{\omega}_B = \tilde{g} = 0$; (b) Dot-dashed (green) curves correspond to $\tilde{\omega}_B = \tilde{g} = 0$, $\tilde{f}_g = 0.3$ for $\tilde{\alpha} = \tilde{\beta} = 0.5$, dashed (blue) curves to $\tilde{\omega}_B = 0.7$, $\tilde{g} = 0$, $\tilde{f}_g = 0$ for $\tilde{\alpha} = \tilde{\beta} = 0.5$, and solid (red) curves to $\tilde{\omega}_B = 0.7$, $\tilde{g} = 0.3$, $\tilde{f}_g = 0$ for $\tilde{\alpha} = 0.5$, $\tilde{\beta} = 0.4$.

in agreement with quantum well width in the experiments [7, 8], $B_0 = 0.9 \text{ T}$ and $B = 0.6 \text{ T}$ (corresponding to $\tilde{\omega}_B = 0.7$), $\tilde{\alpha} = 0.944$ and $\tilde{\beta} = 0.38$ for, e.g. conduction band electron in GaAs with $m^* = 0.068m_0$. Indeed, Rashba SO constant varying in the interval of $\alpha \sim (4.47 - 6.30) \times 10^{-9} \text{ eV} \cdot \text{cm}$ has been reported [17] for InAlAs/InGaAs heterostructures. Furthermore a giant SO splitting was recently observed for quantum well states of a Bi monolayer on Ag(111) [18], on Si(111) [19], and on Cu(001) [20] with Rashba parameters correspondingly $\alpha = 3.05 \times 10^{-8} \text{ eV} \cdot \text{cm}$, $1.37 \times 10^{-8} \text{ eV} \cdot \text{cm}$ and $(1.5 \div 2.5) \times 10^{-8} \text{ eV} \cdot \text{cm}$.

In equilibrium most electrons reside near the bottom E_{k_1} of the lower valley in Fig.4a, which corresponds to an anticrossing point with small effective mass m_1^* and higher mobility μ_1 due to the sharp curvature of the valley. The electric field, applied along k_y axes, bends the Fermi level and accelerates the electrons with a definite (up- or down-) spin polarization to the top of the valley separation E_m when the field reaches a threshold value. The upper valley is more flat where the effective mass m_2^* is rather heavier and the mobility μ_2 is smaller than μ_1 . The ratio m_2^*/m_1^* is estimated to be ~ 80 by fitting the valleys' bottoms to parabolas. Our calculations show that the effective masse in a valley, obtained by anticrossing of a parabola of n th subband with a parabola of $(n+1)$ th subband, can be controlled. Indeed, by changing the signs or the amounts of SO coupling constants, magnetic field, gate voltage and g -factor the bottoms of the parabolas are controllably shifted in different directions along the energy- and momentum-axes, giving different curvatures and effective masses in the valleys. The total electron density n is written as a sum of the densities n_1 and n_2 in the lower and upper valleys, correspondingly, $n = n_1 + n_2$. The population ratio between the upper and lower valleys is assumed to be given by Maxwellian energy distribution

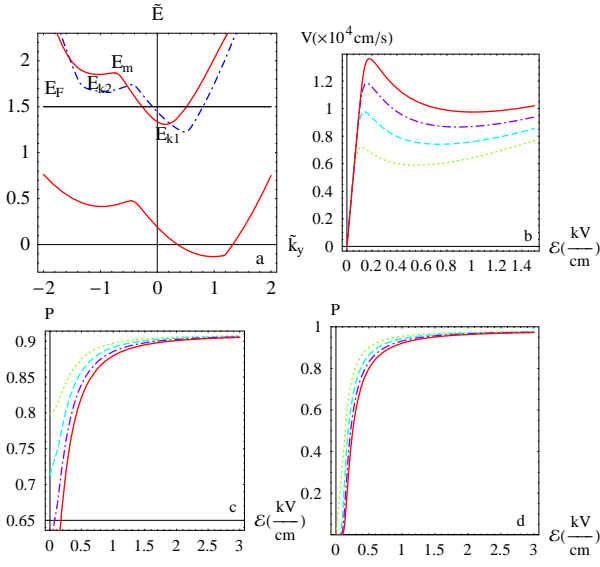


FIG. 4: (Color online) (a) Two valley spectrum corresponding to the lower branch of the first and the second transverse-quantized levels with $\tilde{\alpha} = 0.9$, $\tilde{\beta} = 0.4$, $\tilde{\omega}_B = 0.7$, $\tilde{g} = 0.2$, $\tilde{f}_g = 0$ and $\tilde{k}_x = 0.2$ shown by solid (red) curves, and $\tilde{\alpha} = 1.2$, $\tilde{\beta} = 0.4$, $\tilde{\omega}_B = 0.8$, $\tilde{g} = 0.3$, $\tilde{f}_g = 0.3$ and $\tilde{k}_x = 0.4$ shown by dot-dashed (blue) curve. The dependence of (b) the average drift velocity v and (d) the spin accumulation P on the electric field \mathcal{E} for $\mu_1 = 10 \text{ m}^2/\text{V} \cdot \text{s}$ and $T = 4.2\text{K}$, $\mu = \mu_2/\mu_1 = 0.02$, $R = 50$. (c) P vs. \mathcal{E} for $\mu_1 = 20 \text{ m}^2/\text{V} \cdot \text{s}$ and $T = 50\text{K}$, $\mu = \mu_2/\mu_1 = 0.1$, $R = 10$. Four different values of the activation energy $\Delta E = 4 \text{ meV}$, 6 meV , 8 meV and 10 meV correspond to dotted (green), dashed (violet), dot-dashed (blue), and solid (red) curves in each figures.

as $n_2/n_1 = R \exp(-\Delta E/kT_e)$, where T_e is the electron temperature, R is the ratio of the density of states in the upper N_2 and lower N_1 valleys with $R = m_2^*/m_1^*$ for quasi-2D electron gas, and $\Delta E = E_{k2} - E_{k1}$ is the energy separation between the two valley minima, which can be estimated from e.g. Fig.4a to be $\Delta E = 0.45 \hbar\omega_0$. Then, electron accumulation P with definite spin polarization in the upper valley is written as

$$P = \frac{n_2}{n} = \frac{n_2}{n_1 + n_2} = \frac{R \exp(-\Delta E/kT_e)}{1 + R \exp(-\Delta E/kT_e)}, \quad (4)$$

The electron temperature T_e is defined from the condition $e\mathcal{E}v\tau_e = 3k(T_e - T)/2$, meaning that electrons gain an energy $e\mathcal{E}v\tau_e$ from the electric field \mathcal{E} , aligned in y -axis, as they move up the potential barrier with the average drift velocity $v = (\mu_1 n_1 + \mu_2 n_2)\mathcal{E}/(n_1 + n_2)$, and transfer the excess energy to the atomic lattice with temperature T in the energy relaxation time τ_e , [21]. The steady-state current J is expressed through v as $J = e(\mu_1 n_1 + \mu_2 n_2)\mathcal{E} = env$, which is calculated from the following self-consistent equations

$$T_e = T + \frac{2e\tau_e v \mathcal{E}}{3k}, \quad v = \mu_1 \mathcal{E} \frac{1 + (\mu_2/\mu_1)R \exp(-\Delta E/kT_e)}{1 + R \exp(-\Delta E/kT_e)}. \quad (5)$$

Eqs.(4) and (5) determine completely $v - \mathcal{E}$ or $I - V$ dependence, which displays a shape with a region of

negative differential resistance. Numerical solution of Eqs.(4) and (5) yields a dependence of the spin-polarized electron accumulation P on \mathcal{E} , which is presented in Fig.4c, and d for temperatures $T = 50\text{K}$ and 4.2K , correspondingly. v vs. \mathcal{E} and P vs. \mathcal{E} dependences are depicted in each figures for different valley separations $\Delta E = 4 \text{ meV}$, 6 meV , 8 meV and 10 meV , which are shown by dotted (green), dashed (violet), dot-dashed (blue), and solid (red) curves, respectively. High temperature mobility of electrons in, e.g. GaAs varies in the interval of $(10 \div 20) \text{ m}^2/\text{V} \cdot \text{s}$ [21]. The energy relaxation time τ_e is chosen to be $\tau_e = 10^{-12} \text{ s}$. The higher valley is basically resided at $T = 50\text{K}$ by electrons, according to Fig.4c, due to thermal fluctuations even in the absence of the electric field. The spin-polarized electron accumulation slightly increases from $P \sim 0.6$ up to the saturation value $P \sim 0.90$ as \mathcal{E} increases and reaches $\sim 1.5 \text{ kV/cm}$. The spin-dependent electron accumulation at $T = 4.2\text{K}$, given in Fig.4d for $\mu_1 = 10 \text{ m}^2/\text{V} \cdot \text{s}$, $\mu_2/\mu_1 = 0.02$ and $m_2^*/m_1^* = 50$, sharply increases with electric field from $P \sim 0.0$ up to $P \sim 0.98$ at $\mathcal{E} \sim 1 \text{ kV/cm}$. Fermi energy moves up with increasing the electron concentration and it crosses a subband with opposite spin polarization.

In conclusion, we show that interplay of SO interactions and in-plane magnetic field strongly changes an electron spectrum of quasi-2D electron gas with finite thickness yielding multi-valley energy dispersion in each transverse-quantized subband. As a result, an instable regime of negative differential conductance is realized for spin-polarized electrons.

-
- [1] *Semiconductor Spintronics and Quantum Computation*, Eds. D. D. Awschalom et al. (Springer, Berlin, 2002).
 - [2] E. I. Rashba, *Fiz. Tverd. Tela* (Leningrad) **2**, 1224 (1960) [*Sov. Phys. Solid State* **2**, 1109 (1960)].
 - [3] S. Datta and B. Das, *Appl. Phys. Lett.* **56**, 665 (1990).
 - [4] G. Dresselhaus, *Phys. Rev.* **100**, 580 (1955).
 - [5] O. Chalaev and D. Loss, *Phys. Rev. B* **77**, 115352 (2008).
 - [6] M. Duckheim et al., *Phys. Rev. B* **81**, 085303 (2010).
 - [7] Y. Kato et al., *Science* **299**, 1201 (2003).
 - [8] Y. K. Kato et al., *Phys. Rev. Lett.* **93**, 176601 (2004).
 - [9] E. A. Larid et al., *Phys. Rev. Lett.* **99**, 246601 (2007).
 - [10] E. I. Rashba and Al. L. Efros, *Phys. Rev. Lett.* **91**, 126405; *Phys. Rev. B* **73**, 165325 (2006).
 - [11] V. M. Edelstein, *Solid State Commun.* **73**, 233 (1990).
 - [12] H.-A. Engel, E. I. Rashba, and B. I. Halperin, *Phys. Rev. Lett.* **98**, 036602 (2007).
 - [13] V. Kalevich and V. Korenev, *JETP Lett.* **52**, 230 (1990).
 - [14] R. Lassnig, *Phys. Rev. B* **31**, 8076 (1985).
 - [15] J. B. Gunn, *Solid State Commun.* **1**, 88 (1963).
 - [16] E. I. Rashba, *Physica E* **20**, 189 (2004).
 - [17] L. J. Cui et al., *Appl. Phys. Lett.* **80**, 3132 (2002).
 - [18] C. R. Ast et al., *Phys. Rev. Lett.* **98**, 186807 (2007).
 - [19] I. Gierz et al., *Phys. Rev. Lett.* **103**, 046803 (2009).
 - [20] S. Mathias et al., *Phys. Rev. Lett.* **104**, 066802 (2010).
 - [21] S. M. Sze and Kwok K. Ng, *Physics of Semiconductor Devices*, (John Wiley, New York, 2007) 3rd ed.